

The long-term X-ray variability properties of AGN in the Lockman Hole region

I. E. Papadakis^{1,2}, E. Chatzopoulos¹, D. Athanasiadis³, A. Markowitz⁴, and I. Georgantopoulos³

¹ Physics Department, University of Crete, P.O. Box 2208, GR-710 03 Heraklion, Crete, Greece

² IESL-Foundation for Research and Technology, 711 10 Heraklion, Crete, Greece

³ Institute of Astronomy & Astrophysics, National Observatory of Athens, I. Metaxa & V. Pavlou, GR-152 36 P. Penteli, Athens, Greece

⁴ Center for Astrophysics and Space Sciences, University of California, San Diego, M. C. 0424, LA Jolla, CA 92093-0424, USA

Received ?/ Accepted ?

ABSTRACT

Context. We present the results from a detailed X-ray variability analysis of 66 AGN in the Lockman Hole, which have optical spectroscopic identifications.

Aims. We compare, quantitatively, their variability properties with the properties of local AGN, and we study the “variability – luminosity” relation as a function of redshift, and the “variability – redshift” relation in two luminosity bins.

Methods. We use archival data from the last 10 *XMM-Newton* observations of the Lockman Hole field to extract light curves in the rest frame, 2–10 keV band. We use the “normalized excess variance” to quantify the variability amplitude. Using the latest results regarding the AGN power spectral shape and its dependence on black hole mass and accretion rate, we are able to compute model “variability – luminosity” curves, which we compare with the relations we observe.

Results. When we consider all the sources in our sample, we find that their variability amplitude decreases with increasing redshift and luminosity. These global anti-correlations are less pronounced when we split the objects in various luminosity and redshift bins. We do not find a significant correlation between variability amplitude and spectral slope, Γ . The “variability – luminosity” relation that we detect has a larger amplitude when compared to that of local AGN. We also find that, at a given luminosity, the variability amplitude increases with redshift up to $z \sim 1$, and then stays roughly constant.

Conclusions. Our results imply that the AGN X-ray mechanism operates in the same way at all redshifts. The accretion rate (in units of the Eddington limit) for the objects in our sample increases from ~ 0.25 , at $z \sim 0.5$, to 0.5 at $z \sim 3$. It does not exceed unity even in the case of the most luminous AGN. Their black hole mass also increases with redshift. The upper limit we find is consistent with the largest black hole masses found to date in the local Universe. The black hole mass increase, and the decrease of the rest frame light curve’s duration with increasing redshift, can explain the global variability amplitude – redshift/luminosity anti-correlations that we observe. Among objects with the same luminosity, the black hole mass decreases and the accretion rate increases with larger redshift. This effect explains the increase of the variability amplitude up to redshift ~ 1 (at fixed luminosity bins). At higher redshifts, the decrease of the light curves length affects the variability amplitude significantly, forcing it to remain essentially constant.

Key words. Galaxies: active – X-rays: galaxies

1. Introduction

The X-ray variability properties of nearby AGN have been extensively studied the last twenty years. One of the earliest, and best established so far, result was that the variability amplitude decreases with increasing luminosity (e.g. Barr & Mushotzky 1986; Lawrence & Papadakis 1993; Green et al. 1993; Nandra et al. 1997; Turner et al. 1999; Markowitz & Edelson 2004) although at very low luminosities the anti-correlation breaks, and the variability amplitude drops to nearly zero (e.g. Ptak et al. 1998). This “variability – luminosity” anti-correlation may in fact be the result of a more fundamental “variability – black hole (BH) mass” relation (e.g. Papadakis 2004; O’Neil et al. 2005).

If that is the case, then one could in principle get an estimate of the BH mass from a simple variability amplitude measurement (e.g. Nikolajuk, Papadakis & Czerny 2004; Nikolajuk et al. 2006). Both the “variability – luminosity” and the “variability – BH mass” anti-correlations are probably projections of a “variability – BH mass – accretion rate” fundamental plane (M^cHardy et al. 2006).

The “variability BH mass estimation method” may be important in the case of distant AGN, which have been detected in recent X-ray surveys and in many cases they are too faint in other wavelengths for alternative BH mass estimation methods to apply. However, until recently, knowledge of the X-ray variability properties of distant ($z > 0.1$) AGN was scarce. The situation changed the last few years, when data from deep X-ray surveys become available, and techniques that are able to measure variability amplitudes for low signal-to-noise sources were developed.

Almaini et al. (2000) and Manners et al. (2002) presented the results from an analysis of the X-ray variability of radio-quiet AGN selected from a deep *ROSAT* survey and the *ROSAT* archive, respectively. They confirmed the decline in variability amplitude with luminosity out to redshifts as large as $z \sim 2$. They also noted some evidence for an increase in the variability amplitude at high redshifts. Paolillo et al. (2004) studied the X-ray variability of sources detected in the Chandra Deep Field–South. They also observed an anti-correlation with the luminosity of the sources and, in agreement with the previous studies, they found that high-redshift objects have larger variability amplitudes than expected from extrapolation of their low- z counterparts.

In the current study we measure the variability amplitude of AGN detected by *XMM-Newton* in the Lockman Hole (LH) field. *XMM-Newton* has carried out its deepest survey so far in the direction of this field. Mateos et al. (2005) studied the spectral properties of the 123 brightest sources (i.e. sources more than 500 MOS+PN counts in the 0.2–12 keV band) in this field. Recently, Mateos et al. (2007) presented the results from a detailed study of their flux variability properties as well, using data from 16 of the currently available *XMM-Newton* observations. They found that the variability amplitude does not significantly depend on redshift or X-ray luminosity. They also studied their spectral variability properties, and found that spectral variability is less common than flux variability and a lack of correlation between flux and spectral variability.

In this work we study the variability properties of 66 objects with optical spectroscopic identifications in the LH field, using data from the last 10 *XMM-Newton* observations of the LH field only. These observations were performed over a period of two months on a quasi-regular pattern. As a result, we were able to construct uniformly sampled, high signal-to-noise light curves for all sources in our sample. Furthermore, different to all previous studies, we extracted *rest frame* 2–10 keV band light curves, and we compare, quantitatively, our results with those from the local AGN sample of Markowitz & Edelson (2004). We also quantify the variability amplitude in a way different to what has been used in most cases in the past (i.e. Almaini et al. 2000, Manners et al. 2002, Mateos et al. 2007): we use the “normalized excess variance” a rather well known and frequently used estimator which is easy to interpret.

Our main aim is to study the correlation between the variability amplitude and other source parameters like redshift, X-ray luminosity and X-ray spectral slope and, in particular, to investigate if and how the “variability–luminosity” and “variability – redshift” correlations changes with redshift and luminosity, respectively. Our results suggest that the X-ray source in AGN operates in the same way at all redshifts, and allow us to estimate how the average black hole mass and accretion rate of the AGN in our sample change with redshift.

2. The *XMM-Newton* observations and data reduction

XMM-Newton observed the Lockman Hole field 17 times from April 2000 to December 2002. The total number of X-ray sources detected in this field is 268 (Mateos et al., 2005). Currently, 74 of these objects have been spectroscopically

Table 1. Summary of the 10 LH *XMM-Newton* observations that we used in our study. In the last column we list the “good time interval” (GTI) after the removal of high background periods.

ObsID	Obs. Date	GTI (ksec)
0147510101	2002–10–15	91
0147510801	2002–10–17	75
0147510901	2002–10–19	90
0147511001	2002–10–21	82
0147511101	2002–10–23	50
0147511201	2002–10–25	104
0147511301	2002–10–27	65
0147511601	2002–11–27	100
0147511701	2002–12–04	99
0147511801	2002–12–06	88

identified as either Type I or Type II AGN. They constitute our initial sample of sources. In order to investigate their variability properties we used data from the last 10 *XMM-Newton* observations only. A summary of these observations is reported in Table 1.

By choosing to work with observations which are spread over a period less than two months we minimize the risk that potential changes in the response of the *XMM-Newton* detectors over large period of time will add to the observed variations in the light curves. Furthermore these 10 observations were done in a quasi-regular temporal pattern. The first seven were performed every 2 days over a period of 14 days while the last three over a period of 10 days. Consequently, the choice to use data from these observations only, minimizes differences in the sampling pattern of the resulting light curves.

2.1. Data reduction

During the *XMM-Newton* observations the EPIC PN and MOS cameras were operated in full frame mode with a medium filter. The EPIC data were reprocessed with XMMSPAS version 6.5. We have selected PN photons with PATTERN ≤ 4 (i.e. singles and doubles) and FLAG=0. In the case of the MOS cameras we have selected events with PATTERN ≤ 12 and FLAG=0.

Source counts were accumulated from a circular region of 18'' radius, centered around the coordinates of each source (as listed in Mateos et al. 2005), in the energy range from 2 to 10 keV, in each source’s rest frame. The background count rate, for all EPIC detectors, was determined by accumulating counts from six circular, source free regions, each one of radius 85''. Data from periods of high background were disregarded from further analysis. Given the different redshifts, we constructed the appropriate 2–10 keV background light curves for each source individually. Finally, we produced PN, MOS1 and MOS2, background subtracted, rest frame 2 – 10 keV light curves, for each source in our sample.

Since the *XMM-Newton* EPIC cameras have different geometry, it was common that a number of sources detected in each observation would fall near or inside CCD gaps, and/or close to the edge of at least one of the detectors. Furthermore, in some cases we would detect bad/hot pixels within a source’s photon extraction aperture in one (or more) of the EPIC cameras. For these reasons, we inspected

Table 2. IDs, redshift, spectral and variability properties of the 66 AGN in the Lockman Hole field that we study in this work. The first column lists the source ID as given by Mateos et al. (2005) together with its RA and Dec. Data listed in columns 2, 9, and 10 are taken from Table 8 of Mateos et al. (2005). Numbers in parenthesis in the third column correspond to the 3σ upper limits on σ_{NXS}^2 , in the case of the NV-sources. The values listed in column 9 correspond to the logarithm of the rest frame, 2–10 keV band luminosity of each object. Column 8 indicates whether a light curve is considered as “variable” (V) or “non-variable” (NV) (for details see Section 3.1). Column 11 lists the *XMM-Newton* detectors that were used to construct the respective light curve. The full table is available in electronic form at the CDS.

SourceID	z	σ_{NXS}^2	$\log \sigma_{\text{NXS}}^2$	χ^2/dof	V/NV	$\log(L_X)$	Γ	Instr. Used
5(10 52 43.3 +57 15 45.9)	2.144	0.026±0.015 (0.045)	-1.59±0.26	7.2/4	NV	44.68	1.90	PN
39(10 53 19.09 +57 18 53.6)	0.711	-0.019±0.027 (0.081)	–	1.8/4	NV	43.44	1.79	M1+M2
41(10 51 19.14 +57 18 34.1)	1.640	0.445±0.089	-0.35±0.09	25.5/5	V	44.11	2.06	PN

visually all sources in each PN, MOS1 and MOS2 image. We would also check whether the background count rate we had estimated in an automatic way would be representative of the local background around each source.

As a result of this screening process, light curves from each EPIC detector have a different number of points in most cases. Due to the geometry of the PN detector, the number of sources falling on the PN CCD gaps is larger than the MOS cameras. Consequently, the number of data points, N_{data} , in the PN light curves is usually smaller than the number of points in the MOS light curves.

A reliable estimate of the variability amplitude requires the use of light curves with: a) the largest possible N_{data} and b) the highest signal-to-noise ratio. This ratio can be increased by combining counts from all three EPIC cameras¹. We therefore added the background subtracted PN and MOS light curves to create combined PN+MOS1+MOS2, PN+MOS1, PN+MOS2 and MOS1+MOS2 light curves. Among the individual and combined light curves of each source we would finally choose the one with the largest number of points. In the case there were more than one, we would choose the light curve with data taken from as many as possible EPIC detectors.

The largest N_{data} value among all light curves is eight. Since N_{data} (and hence the sampling pattern as well) should be roughly the same in all of them, we required that $N_{\text{data}} \geq 4$ (i.e. half of $N_{\text{data,max}}$). There are 66 (out of the 74) AGN whose light curves satisfy this criterion. These sources constitute our final sample. Table 2 lists their ID number, redshift, X-ray spectrum slope, Γ , and rest frame, 2–10 keV band luminosity, L_X . In the last column of the same Table we list the combination of the EPIC cameras that we used for each source.

There is just one object with $N_{\text{data}} = 4$ in our sample, and four with $N_{\text{data}} = 8$. In most cases, $N_{\text{data}} = 6$. Due to this fact, the sampling pattern of most light curves is indeed similar, in the *observer’s frame*. However, when one

¹ One must be careful in combining data from the three EPIC cameras, given the difference in their response. However, the uncertainty introduced to our results by the difference in the average energy of the (rest frame) 2–10 keV band photons in the EPIC PN, MOS1 and MOS2 cameras is smaller than that introduced by say the small number of points in the light curves and the (unknown) stochastic nature of the underlying variability process. For this reason, we use light curves with photons accumulated from as many cameras as possible, as explained in the text.

takes into account the different redshifts of the sources in our sample, the light curves’ duration changes, from one source to the other, in their *rest frame*. This redshift induced inhomogeneity in the temporal pattern of the light curves has to be taken into account when we compare and interpret the variability properties of the low and high- z objects in our sample.

3. Variability analysis method

3.1. Detection of intrinsic flux variations

First we investigated which light curves show significant variations, using the χ^2 test. Since our sample consists of the brightest sources in the catalogue of Mateos et al. (2005), there are more than 15 source photons in each point of their light curves. This guarantees the applicability of Gaussian statistics, and hence the reliability of the χ^2 test results. The results ($\chi^2/\text{degrees of freedom}$) are listed in the 7th column of Table 2. We accept that a source shows significant flux variations if the probability of χ^2 being larger than the obtained value, by chance, is smaller than 5%. Column 8 on the same table lists whether a source is variable (“V”) or not (“NV”), according to this criterion².

Sixteen objects, i.e. 24% of the sources in the sample, turned out to be non variable. In order to investigate this issue further, we used the Kolmogorov-Smirnov (K–S) test to compare the distribution functions of the redshift, N_{data} and mean count rate (CR) of the V and NV-subsamples.

We find that the redshift distribution functions of the two subsamples are almost identical. However, we get a different view when we consider the results from the comparison of the CR and N_{data} distributions. The NV-sources are systematically fainter than the V-sources. We find that $\langle \text{CR}_{\text{NV}} \rangle = 7.1 \times 10^{-4}$ cnts/s and $\langle \text{CR}_{\text{V}} \rangle = 2.2 \times 10^{-3}$ cnts/s. The K–S test suggests that the difference in brightness is significant at the 96% level. There are also less points in the light curves of the NV-sources. We find that $\langle N_{\text{data,NV}} \rangle = 5.7$ as opposed to $\langle N_{\text{data,V}} \rangle = 6.2$. The K–S test suggests that the difference in the distribution of N_{data} is significant at the 99.94% level. We conclude that we do not detect intrinsic variations in the NV-sources most probably because they are less bright and their light curves have fewer points than the V-sources.

² In the Appendix we discuss in detail the possibility that the observed variations may be affected significantly by instrumental effects

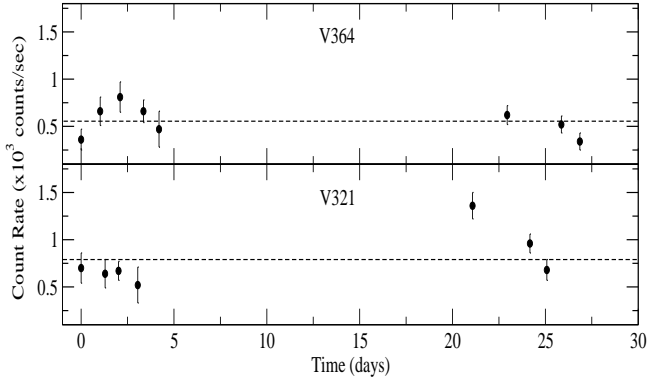


Fig. 1. The rest frame, 2–10 keV light curve of source V364, which is a “NV” object, and V321, which belongs in the “V” subsample. Time is measured in days (in rest frame) since the first observation of each source.

Fig. 1 shows the rest frame, 2–10 keV light curve of the objects with ID numbers V364 and V321. Their average count rate is similar, and in fact there are more points in the V364 light curve. Nevertheless, it is source V321 which shows significant variations in its light curve. As Fig. 1 shows this is due to just one point (which we have carefully examined to establish its reliability). This result demonstrates clearly the importance of working with light curves which have the largest possible number of points (and justifies the way we constructed the light curves, as explained in the previous section).

3.2. Determination of variability amplitude

We use the normalized excess variance, σ_{NXS}^2 (e.g. Nandra et al. 1997) as a measure of the intrinsic variability amplitude of the light curves. This estimator is defined as,

$$\sigma_{\text{NXS}}^2 = \frac{S^2 - \langle \sigma_{\text{err}}^2 \rangle}{\langle x \rangle^2}, \quad (1)$$

where $\langle x \rangle$, and $S^2 = (1/N_{\text{data}}) \sum_{i=1}^{N_{\text{data}}} (x_i - \langle x \rangle)^2$ are the mean and variance of the light curve, while $\langle \sigma_{\text{err}}^2 \rangle = (1/N_{\text{data}}) \sum_{i=1}^{N_{\text{data}}} \sigma_{\text{err},i}^2$ is the average contribution of the Poisson noise process to the observed scatter around the mean. Its square root (F_{var}) indicates the average variability amplitude of a source as a fraction of its light curve mean.

The spread of the observed σ_{NXS}^2 values around the intrinsic, “true” σ^2 value (i.e. the “error” of σ_{NXS}^2) should decrease with increasing N_{data} . This spread also depends on the stochastic nature of the process underlying the AGN X-ray variability (see Vaughan et al. 2003 for a detailed discussion on this issue). In fact, even if a source is not intrinsically variable, the σ_{NXS}^2 estimates based on light curves from observations performed at different times will not be identical, due to the presence of the Poisson noise alone.

It is not easy to estimate a priori how does the error on σ_{NXS}^2 depend on N_{data} and on the stochastic nature of the variability mechanism. On the other hand, the error due to Poisson noise can be estimated using the following equation (Vaughan et al. 2003),

$$\text{err}(\sigma_{\text{NXS}}^2) = \sqrt{\frac{2}{N_{\text{data}}} \left(\frac{\langle \sigma_{\text{err}}^2 \rangle}{\langle x \rangle^2} \right)^2 + \frac{\langle \sigma_{\text{err}}^2 \rangle}{N_{\text{data}}} \frac{4\sigma_{\text{NXS}}^2}{\langle x \rangle^2}}. \quad (2)$$

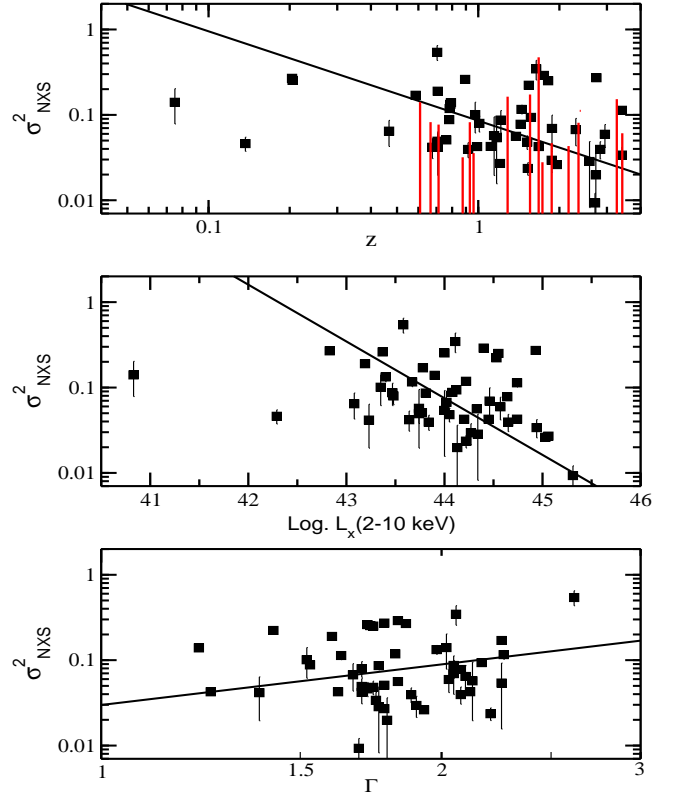


Fig. 2. Plot of σ_{NXS}^2 as a function of redshift (top panel), logarithm of the rest-frame 2–10 keV luminosity (middle panel) and spectral slope value (bottom panel), for the 50 variable sources in our sample. The vertical gray lines in the top panel show the 3σ upper limits on σ_{NXS}^2 in the case of the NV-sources.

This is useful in order to estimate upper limits on the intrinsic excess variance in the case when we do not detect significant variations.

Columns 3 and 4 in Table 2 list the excess variance, and its error, for all the sources in our sample. In the case of the NV-sources, σ_{NXS}^2 is consistent with zero, as expected. For these sources, the numbers in parenthesis in the third column correspond to the 3σ upper limits, i.e. $\sigma_{\text{NXS}}^2 + 3\text{err}(\sigma_{\text{NXS}}^2)$. In columns 5 and 6 we list the logarithm of σ_{NXS}^2 and its error, estimated using the usual “propagation of errors” formula.

4. Correlation of variability amplitude with source parameters

We now proceed to study the correlation between the excess variance and source parameters such as the redshift, L_X , and Γ . In order to quantify the correlation between two parameters, we use the Kendall’s τ rank correlation coefficient. We accept a correlation to be significant if the null hypothesis probability, P_{null} , is less than 5%.

Filled squares in the upper panel of Fig. 2 show the “ σ_{NXS}^2 vs z ” plot for the 50 variable sources in our sample. Errors are estimated using equation (2). A trend of decreasing variability amplitude with increasing redshift can be seen. When we consider the $[\log(\sigma_{\text{NXS}}^2), \log(z)]$ data for the variable sources only, we find that $\tau = -0.2$, a result

which confirms the significance of the “variability – z ” anti-correlation ($P_{\text{null}} = 0.04$).

The vertical grey lines in the same panel of Fig. 2 show the 3σ upper limits on σ_{NXS}^2 in the case of the NV-sources. They are so large that they do not impose any significant constraints on the “ $\sigma_{\text{NXS}}^2 - z$ ” relation. We need better light curves for these objects (in terms of signal-to-noise ratio and N_{data}) to constrain this relation better. The same holds true for all relations we study below. For that reason, we do not consider hereafter the NV-sources in our analysis.

The solid line in the same figure shows the best fitting, “ordinary least squares bisector” line to the data in log-log space (the best fitting parameter values were estimated as in Isobe et al. 1990). We find that a relation of the form $\sigma_{\text{NXS}}^2 \propto z^{-\alpha}$, with $\alpha = -1.05 \pm 0.10$ fits the data well.

Next, we examined the relation between variability amplitude and L_X . The middle panel in Fig. 2 shows the “ σ_{NXS}^2 vs $\log(L_X)$ ” plot for the V-objects in our sample. Given the correlation between L_X and redshift, it is not surprising that we an anti-correlation between variability amplitude and luminosity can be seen. Kendall’s τ suggests that the anti-correlation between $\log(\sigma_{\text{NXS}}^2)$ and $\log(L_X)$ is significant ($\tau = -0.22$, $P_{\text{null}} = 0.023$). The solid line shows the best fitting $\sigma_{\text{NXS}}^2 \propto L_X^{-\alpha}$ line ($\alpha = -0.66 \pm 0.12$), which fits the data rather well.

In the bottom plot we show the “ σ_{NXS}^2 vs Γ ” relation for the V-sources in our sample. One could perhaps suggest a positive correlation between the two quantities, but Kendall’s τ in this case does not support this claim ($\tau = 0.03$, $P_{\text{null}} = 0.74$). The best fitting $\sigma_{\text{NXS}}^2 \propto \Gamma^{-\alpha}$ model to the data ($\alpha = 1.58 \pm 1.14$) is also shown with the solid line. The uncertainty is so large that the possibility of $\alpha = 0$ (i.e. of no correlation between σ_{NXS}^2 and Γ) cannot be excluded.

The “ $\sigma_{\text{NXS}}^2 - \log(L_X)$ ” anti-correlation that we find is in agreement with what has been observed in nearby AGN, both on long time scales (e.g. Papadakis 2004; Markowitz & Edelson, 2004) and short time scales (e.g. O’ Neil et al. 2005, and references therein). In fact our results indicate that the decline in variability amplitude with luminosity holds out to redshifts as high as ~ 3 . This decline can also explain the “ $\sigma_{\text{NXS}}^2 - z$ ” anti-correlation: as the more distant objects are systematically more luminous, it is not surprising that they are also less variable. However, it is important to note here that, although the correlations we detect are statistically significant, they are also driven by a few individual points. For example, if we omit the high- z source with $\sigma_{\text{NXS}}^2 < 0.01$ then $P_{\text{null}} > 0.05$ in the case of the $[\log(\sigma_{\text{NXS}}^2), \log(z)]$ anti-correlation. We reach the same conclusion if we omit the two points with the smallest σ_{NXS}^2 in the case of the $[\log(\sigma_{\text{NXS}}^2), \log(L_X)]$ anti-correlation. Consequently, one has to be careful regarding the reality of these correlations.

5. Comparison with nearby AGN

In this section we present the results from a quantitative comparison between the “variability – luminosity” relation as determined for nearby AGN and the V-objects in our sample, grouped in various redshift bins. We use the Student’s- t test to compare the mean of two sample distributions. We consider two means as being significantly different if P_{null} is smaller than 5%.

In order to determine the “ $\log(\sigma_{\text{NXS}}^2)$ vs $\log(L_X)$ ” relation for the AGN in the local universe we considered the 12 objects in the sample of Markowitz & Edelson (2004). Object names and the dates of the *RXTE* observations that were used to extract light curves are listed in Table 1 of Markowitz & Edelson (2004). Details of the data reduction can also be found in the same paper.

Filled squares in all panels of Fig. 3 show the $[\log(\sigma_{\text{NXS}}^2), \log(L_X)]$ data of these AGN. Excess variances were estimated as described in Section 3.2. In the case when there were more than one light curves for an object, we plot the straight mean of the individual σ_{NXS}^2 values. We used 1.6 days binned, 2–12 keV light curves, which were 23.2 days long. This is equal to the average, rest frame light curve length of the V-sources in our sample. As for L_X , we adopted the 2 – 12 keV luminosity measurements of Markowitz & Edelson (2004). This is slightly different to the energy band we chose in this work, but this should not affect our results significantly.

The open circles in the top, middle and bottom panel of Fig. 3 show the $[\log(\sigma_{\text{NXS}}^2), \log(L_X)]$ data of the V-sources with $0.2 < z < 1$ (the “Low”-redshift bin; 18 objects), $1 < z < 2$ (“High”-redshift bin; 21 objects) and $2.3 < z < 3.4$ (“very High”, or vHigh, redshift bin; 9 objects). The average redshift of the objects in the Low- z , High- z and v-High bins is $\langle z_{\text{Low-}z} \rangle = 0.7$, $\langle z_{\text{High-}z} \rangle = 1.48$ and $\langle z_{\text{vHigh-}z} \rangle = 2.85$.

In order to reduce the scatter of the Low- z data points in Fig. 3, we sorted them in order of increasing luminosity, we considered three bins of 6 points each, and we estimated their average $\log(\sigma_{\text{NXS}}^2)$ and $\log(L_X)$ values (shown with filled circles in the top panel of Fig. 3). Similarly, filled circles in the middle panel show the mean $\log(\sigma_{\text{NXS}}^2)$ and $\log(L_X)$ values of the data in three bins (each of 7 points) into which we grouped the High- z objects (in order of increasing luminosity). We also binned the vHigh- z objects in two groups and we estimated their average $\log(\sigma_{\text{NXS}}^2)$ and $\log(L_X)$ values. The results are shown with the filled circles in the bottom panel of Fig. 3.

On average, Low- z and nearby AGN have similar X-ray luminosity. We find that $\langle \log(L_{X,\text{Low-}z}) \rangle = 43.62$ as opposed to $\langle \log(L_{X,\text{nearby}}) \rangle = 43.31$ ($P_{\text{null}} = 0.21$). On the other hand, the High- z and vHigh- z AGN are significantly more luminous than the nearby AGN: $\langle \log(L_{X,\text{High-}z}) \rangle = 44.24$ and $\langle \log(L_{X,\text{vHigh-}z}) \rangle = 44.63$ ($P_{\text{null}} = 4 \times 10^{-4}$, and $P_{\text{null}} = 7.3 \times 10^{-4}$, respectively). If both the LH and the nearby AGN followed the same “ $\sigma_{\text{NXS}}^2 - \log(L_X)$ ” relation, we would expect the Low- z objects to be as variable as the nearby AGN, and the High- z and vHigh- z AGN to be significantly less variable. However, this is not the case.

The average variability amplitude of the nearby and the Low- z AGN are $\langle \log(\sigma_{\text{NXS},\text{nearby}}^2) \rangle = -1.45$ and $\langle \log(\sigma_{\text{NXS},\text{Low-}z}^2) \rangle = -0.97$. We find that their difference is significant ($P_{\text{null}} = 0.003$). Even the High- z sources are significantly more variable than the nearby AGN ($\langle \log(\sigma_{\text{NXS},\text{High-}z}^2) \rangle = -1.13$, $P_{\text{null}} = 0.031$), while the vHigh- z objects are at least as variable as the nearby AGN, despite the fact that they are much more luminous ($\langle \log(\sigma_{\text{NXS},\text{vHigh-}z}^2) \rangle = -1.34$, $P_{\text{null}} = 0.57$).

We conclude that, at a given X-ray luminosity, the $z > 0.2$, V-sources in our sample are systematically more variable than the nearby AGN. This is in agreement with the results of Almaini et al. (2002), who found that the

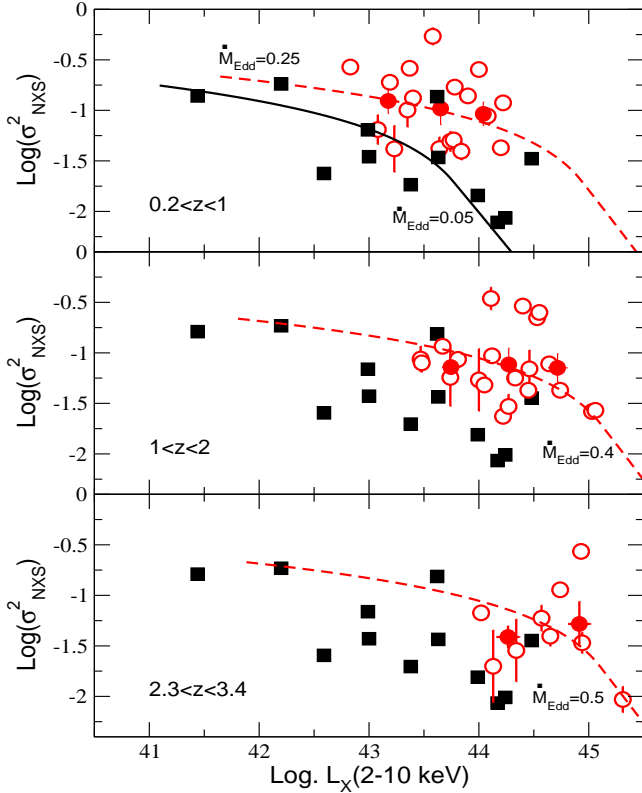


Fig. 3. The “variability – luminosity” plot for the nearby AGN (filled squares in all plots), the Low- z , High- z and vHigh- z objects in the V-subsample (open circles in the top, middle and bottoms panels, respectively). Filled, grey circles correspond to the mean variability amplitude and luminosity, when data are grouped in various bins as explained in the text. The solid line in the top panel and the long-dashed lines in all panels show the model “variability amplitude – $\log(L_X)$ ” lines, estimated as explained in Section 6.

$z > 0.5$ AGN do not show the anti-correlation with luminosity seen in local AGN, and the results of Paolillo et al. (2004), who found that high- z objects have larger variability amplitudes than expected from extrapolations of their low- z counterparts.

6. Impact of BH mass and accretion rate to the variability – luminosity relation

Let us assume that the X-ray variability mechanism is the same in all AGN, irrespective of their redshift. This assumption implies that the power spectral density, PSD, has the same shape in all of them. Recent work, based on detailed analysis of high quality *RXTE* and *XMM-Newton* light curves, has shown that the AGN PSDs have a power-law shape of slope ~ -2 for the 2–10 keV band (as opposed to ~ -2.7 for softer bands), which changes to a slope of ~ -1 below a so-called “break frequency”, ν_{bf} (e.g. Markowitz et al., 2003; McHardy et al., 2004).

The excess variance estimated from a light curve of length T , is an approximate estimator of the following integral,

$$\sigma_{\text{NXS}}^2 = \int_{\nu_{lf}}^{\infty} \text{PSD}(\nu) d\nu, \quad (3)$$

where $\nu_{lf} = 1/T$. If, as we assumed above, $\text{PSD}(\nu) = A(\nu/\nu_{bf})^{-1}$ ($\nu < \nu_{bf}$) and $\text{PSD}(\nu) = A(\nu/\nu_{bf})^{-2}$ (when $\nu > \nu_{bf}$), then,

$$\sigma_{\text{NXS}}^2 = \text{PSD}_{\text{amp}} [\ln(\nu_{bf}) - \ln(\nu_{lf}) + 1], \quad (4)$$

where $\text{PSD}_{\text{amp}} = A\nu_{bf} \sim 0.02$ (Papadakis 2004). In the case when $\nu_{lf} > \nu_{bf}$,

$$\sigma_{\text{NXS}}^2 = (\text{PSD})_{\text{amp}} (\nu_{bf}/\nu_{lf}). \quad (5)$$

Recently, McHardy et al. (2006) have demonstrated that ν_{bf} depends on both the BH mass, M_{BH} , and the accretion rate, \dot{m}_{Edd} (measured in Eddington units), as follows,

$$\nu_{bf} = 0.029\eta\dot{m}_{\text{Edd}}(M_{\text{BH}}/10^6M_{\odot})^{-1}, \quad (6)$$

where η is the efficiency of the mass to energy conversion (hereafter we assume $\eta = 0.1$). One can now use the above equation to substitute ν_{bf} in equations 4 and 5 in order to relate σ_{NXS}^2 with M_{BH} and \dot{m}_{Edd} . The resulting relation implies that for a given M_{BH} , σ_{NXS}^2 increases with increasing accretion rate, while, among all AGN with the same \dot{m}_{Edd} , objects with smaller M_{BH} should have larger variability amplitude.

The $\sigma_{\text{NXS}}^2 = f(M_{\text{BH}}, \dot{m}_{\text{Edd}})$ relation can be transformed to a $\sigma_{\text{NXS}}^2 = f(L_X)$ relation if we use the fact that the bolometric luminosity, L_{bol} , is given by $L_{\text{bol}} = 1.3\eta\dot{m}_{\text{Edd}}10^{39}(M_{\text{bh}}/M_{\odot})$ erg/s, and we adopt an X-ray luminosity to L_{bol} conversion factor. To this end, we adopted the Marconi et al. (2004) prescription,

$$\log(L_X) = \log(L^*) - 1.54 - 0.24\ell - 0.012\ell^2 - 0.0015\ell^3, \quad (7)$$

where $\ell = \log L^* - 12$, L^* being the bolometric luminosity in solar luminosity units.

To summarize, it is possible to derive a model “ σ_{NXS}^2 vs L_X ” relation, if we assume that: 1) all AGN, at all redshifts, vary like the local AGN, 2) the efficiency is the same in all objects, and 3) a bolometric to X-ray luminosity conversion relation. In addition, the model takes into account the different *rest frame* length of the derived light curves (“the redshift induced inhomogeneity” we mentioned in Section 2). Although T_{obs} is similar in all light curves, ν_{lf} in equations (4) and (5) should be equal to $1/T_{\text{restframe}}$, where $T_{\text{restframe}} = T_{\text{obs}}/(1+z)$.

The solid line in the upper panel of Fig. 3 shows such a model “ $\log(\sigma_{\text{NXS}}^2)$ vs $\log(L_X)$ ” curve in the case when $\dot{m}_{\text{Edd}} = 0.05$ and $\nu_{lf, \text{nearby}} = 1/23.2 \text{ days}^{-1}$. Clearly, this line describes rather well the “variability – luminosity” relation for the nearby AGN. This is not surprising given the fact that the model PSD shape that we have assumed, and the “ ν_{bf} vs BH mass and accretion rate” relation that we use, have resulted from the study of objects which are all included in our nearby AGN sample.

The long dashed line in the same panel show the model “ $\log(\sigma_{\text{NXS}}^2)$ vs $\log(L_X)$ ” relation in the case when $\dot{m}_{\text{Edd}} = 0.25$ and $\nu_{lf} = 1/29.6 \text{ days}^{-1}$ (29.6 days is the average, rest frame duration of the Low- z light curves). This is entirely consistent with the mean $[\log(\sigma_{\text{NXS}}^2), \log(L_X)]$ data of the Low- z objects.

The model curves plotted in the upper panel of Fig. 3 can be used to explain the differences we observe between the nearby and Low- z AGN. For example, let us consider

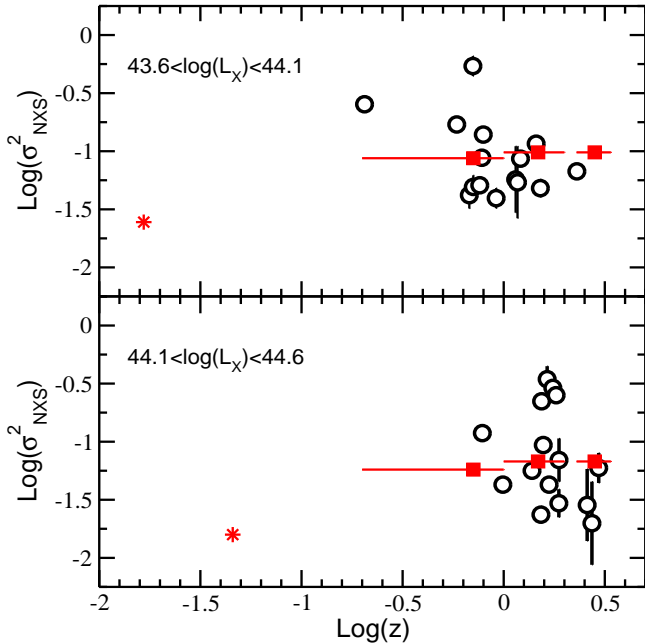


Fig. 4. The “variability – redshift” relation for the variable sources in our sample with “low” and “high” luminosity (open circles in the top and bottom panels, respectively). Filled squares show the model predictions, estimated as explained in Section 6.1, and stars indicate the average variability amplitude and redshift of the “lowLum” and “highLum”, nearby AGN.

the objects with $\log(L_X) = 44$. According to the model, in the local Universe these are objects with $\log(M_{\text{BH}}) \sim 8.7$ and $\dot{m} \sim 5\%$ of the Eddington limit. The fact that the respective Low- z sources are more variable can be explained by a smaller black hole mass ($\log(M_{\text{BH}}) \sim 8$) and a higher accretion rate ($\dot{m} \sim 25\%$ of the Eddington limit). At the same time, the higher accretion rate compensates the difference in BH mass, and explains why objects with different BH mass have the same luminosity.

The long dashed lines in the middle and bottom panels of Fig. 3 show the model “ $\log(\sigma_{\text{NXS}}^2)$ vs $\log(L_X)$ ” lines for $\dot{m}_{\text{Edd,High-}z} = 0.4$, $\dot{m}_{\text{Edd,vHigh-}z} = 0.5$, $\nu_{lf,\text{High-}z} = 1/20.2$ days $^{-1}$ and $\nu_{lf,\text{vHigh-}z} = 1/12.7$ days $^{-1}$ (20.2 and 12.7 days being the average, rest-frame length of the High- z and vHigh- z light curves, respectively). Clearly, these model curves describe well the mean variability amplitude vs X-ray luminosity data of these objects.

6.1. The “variability – redshift” relation in AGN

According to the model presented above, as the redshift increases, objects at a given luminosity bin should correspond to AGN of smaller BH mass (hence the larger variability amplitude) and higher accretion rate. Therefore, we would expect the variability amplitude of AGN with the same luminosity to increase with increasing redshift. In order to investigate this issue further, we considered the “variability – redshift” relation at fixed luminosity bins.

Open circles in Fig. 4 shows the $[\log(\sigma_{\text{NXS}}^2), \log(z)]$ data for the variable objects in our sample with $L_X = 10^{43.6} - 10^{44.1}$ ergs/s (top panel; the “lowLum” bin) and $L_X = 10^{44.1} - 10^{44.6}$ ergs/s (bottom panel; the “highLum”

bin). Star-like points in both panels show the average variability amplitude and redshift for the nearby, “lowLum” and “highLum” AGN. Contrary to the “variability – redshift” anti-correlation we detect when we consider all variable sources together (see top panel in Fig. 2), here one can even claim a positive correlation between σ_{NXS}^2 and redshift: the variability amplitude of the higher redshift, LH AGN is higher than the amplitude of the nearby objects with the same luminosity. This is in agreement with the discussion in the paragraph above.

However, the situation is less clear when we consider the LH sources only (i.e. the AGN at redshift larger than ~ 1 or so). We find that there does not exist a significant anti-correlation (or correlation) either in the “low” or “highLum” bins ($\tau_{\text{lowLum}} = -0.16$, $\tau_{\text{highLum}} = -0.17$, with $P_{\text{null,lowLum}} = 0.4$, and $P_{\text{null,highLum}} = 0.37$, respectively).

The average X-ray luminosity of the lowLum and highLum sources is $< \log(L_{X,\text{lowLum}}) > = 43.8$ and $< \log(L_{X,\text{highLum}}) > = 44.3$. We can now use the $\dot{m}_{\text{Edd}} = 0.25, 0.4$ and 0.5 model curves, shown with the dashed lines in Fig. 3, to estimate the amplitude of objects with $L_X = 10^{43.8}$ and $L_X = 10^{44.3}$ ergs/s in the Low- z , High- z and vHigh- z redshift bins, respectively. Filled (grey) squares in Fig. 4 show the variability amplitude of these objects (as x-axis coordinates we have used the average redshift of all sources in the Low- z , High- z and vHigh- z bins, while the horizontal bars correspond to the size of the respective bins). Clearly, the model “variability - redshift” relations agree well with the data in both luminosity bins.

The main reason that we do not observe a strong, positive correlation between variability amplitude and redshift (when $z > 1$) at fixed luminosity bins is that, the rest frame light curve length, $T_{\text{restframe}}$, and hence σ_{NXS}^2 as well, decreases with increasing redshift. Therefore, although the more distant AGN have a smaller BH mass and higher accretion rate than the local, same luminosity objects, their variability amplitude is not as large as we would expect due to this decrease in $T_{\text{restframe}}$. This “ $T_{\text{restframe}}$ – redshift” anti-correlation is strong enough to compensate the increase in σ_{NXS}^2 due to the higher \dot{m}_{Edd} and smaller M_{BH} .

7. Discussion and conclusions

We have studied the long term X-ray variability properties of 66 AGN in the Lockman Hole field which have optical spectroscopic identifications. We used rest frame 2–10 keV band light curves, and we have taken particular care that they all have a similar sampling pattern. For this reason, we extracted data from the last 10 *XMM-Newton* observations of this region only, and we restricted our sample to objects with $N_{\text{data}} \geq 4$.

Using the χ^2 test, we detected significant variations in 50 of them. The low signal-to-noise ratio and the smaller number of points in the light curves of the remaining 16 objects can explain the absence of significant variations in them. We have used the well known “normalized excess variance”, σ_{NXS}^2 , estimator in order to quantify the variability amplitude of these AGN. We have also used *RXTE* light curves of 12 nearby AGN, with an average energy and length similar to the LH AGN, in order to measure their normalized excess variance and compare their variability properties with the Lockman Hole AGN. Our results can be summarized as follows:

a) When we consider all the objects in our sample together, we detect a significant anti-correlation between redshift, luminosity and variability amplitude: the amplitude decreases with increasing redshift and luminosity. This “variability – luminosity” anti-correlation is in agreement with (and extends out to redshift of ~ 3) the results of Almaini et al. (2000), Manners et al. (2002) and Paolillo et al. (2004).

b) We do not find a significant correlation between variability amplitude and Γ . This is in agreement with the results of Mateos et al. (2007) but opposite to what has been observed in nearby AGN, where sources with steeper spectra show larger amplitude variations (e.g. Green et al. 1993, Turner et al. 1999, Grupe et al. 2001). Paolillo et al. (2004) also observed sources with harder energy spectra to be less variable in their study of the X-ray variability properties of the AGN in the *Chandra* Deep Field-South. In order to investigate this issue further, we searched for a “variability – Γ ” relation in the Low- z , High- z and vHigh- z subsamples, but we did not detect any. Perhaps, if real, such a “variability – spectral shape” correlation has such a large intrinsic scatter, in which case we would need a larger sample to detect it.

c) The “variability – luminosity” relation of the Lockman Hole AGN has a larger amplitude when compared to that of local AGN. This is in agreement with the results of Almaini et al. (2000), Manners et al. (2002) and Paolillo et al. (2004), who also found that high-redshift sources behave differently, in terms of their variability amplitude, than their nearby counterparts.

d) The global “variability amplitude–redshift/luminosity” anti-correlations are less pronounced when we consider AGN in various luminosity and redshift bins. The main trend we detect is that, at a given luminosity bin, the variability amplitude increases with redshift until $z \sim 1$, and then stays roughly constant.

It is not possible to compare quantitatively our results with those presented in the past. Quantitative comparisons can be performed when one uses light curves of similar duration and rest frame energy band. Furthermore, the variability amplitude must be measured in the same way, preferably with the use of an estimator whose relation with the AGN fundamental physical parameters, like the BH mass and accretion rate, can be established. Such an estimator is the “normalized excess variance”, which we adopted in this work, since its dependence on M_{BH} , \dot{m}_{Edd} and the light curve’s length can be easily determined (Section 6.1).

In any case, we believe that parameters like the slope of the best fitting line in the overall “variability–luminosity” or “variability – redshift” plots (top and middle panels in Fig. 2) do not provide important physical insights. The shape of the “variability–luminosity/redshift” relations is strongly affected by factors like the length of the light curves used and their energy band. Such “experimental” parameters can introduce or even “destroy” any global “variability–luminosity” or “variability – redshift” anti-correlations. For example, as we discussed in Section 4, although formally significant, the “variability–luminosity” and “variability – redshift” anti-correlations that we detect are mainly driven by a few points. A better understanding of how the AGN variability properties change with look-back time can be achieved by studying the “variability–luminosity” and/or the “variability–redshift” relations in small, fixed redshift and luminosity bins, respectively.

Our results are fully consistent with the assumption that the X-ray variability mechanism and the accretion efficiency are the same in all AGN, at all redshifts. In other words, our results strongly suggest that the X-ray source operates in the same way in all AGN, at all redshifts. We find that, as the redshift increases, same luminosity AGN have smaller BH mass and higher accretion rates. At the same time, as the redshift increases, the rest frame light curve length decreases accordingly. For this reason the variability amplitude (for the same luminosity AGN) increases slightly up to $z \sim 1$, and then remains roughly constant with redshift.

On the other hand, in the overall “variability amplitude–redshift/luminosity” plots (shown in Fig. 2) the high luminosity objects are mainly those with the highest redshift as well. According to our results, their accretion rate should be the highest among the sources in our sample. Consequently, they should also show a large variability amplitude. However, they also have large BH masses, and their *rest frame* light curve length is also small. These two effects reduce significantly the observed variability amplitude, and can explain the global anti-correlation we observe between variability and redshift/luminosity.

7.1. BH mass and accretion rate estimation

To the extent that all AGN vary like the nearby ones (as our results suggest), we can provide BH mass and accretion rate estimates for the objects in our sample. Obviously, given the large scatter of the σ_{NXS}^2 values, such a measurement will not be very accurate if it were to be quoted individually for each object in our sample. The variability method can only provide *average* estimates of M_{BH} and \dot{m}_{Edd} .

Even in this case, these estimates can only be considered as indicative at this point. For example, the largest number of sources (21) are in the “Low- z ” bin. The $\dot{m}_{\text{Edd}} = 0.4$ model curve in the middle panel of Fig. 2 appears to agree well with the average $[\log(\sigma_{\text{NXS}}^2), \log(L_{\text{X}})]$ points in this bin, but this is hard to quantify. With just 3 points to compare with, we cannot perform a proper χ^2 fit to judge the goodness of the model fit and provide confidence ranges for the best-fitting model parameter values. We need significantly larger samples of high- z AGN, in order to improve the accuracy of our results.

Having these comments in mind, the model curves in Fig. 3 suggest that, on average, the Low ($z \sim 0.7$), High ($z \sim 1.5$) and vHigh- z ($z \sim 2.9$) Lockman Hole AGN accrete at $\sim 25, 40$ and 50% of the Eddington limit. Our results are in agreement with those of McLure & Dunlop (2004) who also observe a slow evolution of the Eddington ratio from $\dot{m}_{\text{Edd}} \sim 0.15$ at $z \sim 0.2$ to $\dot{m}_{\text{Edd}} \sim 0.5$ at $z \sim 2$, for a large sample of quasars drawn from the SDSS catalogue. Although a few objects in Fig. 3 show variability amplitudes well above the average (by a factor up to 10 in some cases), these outliers are probably of stochastic nature (notice for example that the scatter of points at a given luminosity in the middle panel of Fig. 2 is of a similar magnitude). We conclude that, most probably, the majority of the sources in our sample are accreting at rates below the Eddington limit. This limit seems to be a relevant physical boundary to the AGN accretion rate out to redshift ~ 3 .

Regarding black hole masses, the model curves in Fig. 3 suggest a BH mass range of $5 \times 10^6 - 2 \times 10^8 M_{\odot}$ in the case of the Low- z objects, $1.5 \times 10^7 - 6.6 \times 10^8 M_{\odot}$ for the

High- z objects, and $5 \times 10^7 - 1.3 \times 10^9 M_{\odot}$ for the AGN in the vHigh- z bin. Interestingly, even for these high- z and very luminous objects, the highest BH mass estimate is less than $3 \times 10^9 M_{\odot}$, i.e. the most massive BH measured dynamically in the local Universe and the expected BH mass limit based on the known properties of early-type galaxies and the locally observed correlation between bulge and black hole mass (McLure & Dunlop, 2004).

References

- Almaini, O., Lawrence, A., Shanks, T. et al. 2000, MNRAS, 315, 325
 Barr, P. & Mushotzky, R.F. 1986, Nature, 320
 Edelson, R. A. & Krolik, J. H. 1988, ApJ, 333, 646
 Green, A.R., McHardy, I.M. & Lehto, H.J. 1993, MNRAS, 265, 664
 Grupe, D., Thomas, H.-C. & Beuermann, K. 2001, A&A, 367, 470G
 Isobe, T., Feigelson, E.D., Akritas, M.G. & Babu, G.J. 1990, ApJ, 364, 104I
 Lawrence, A. & Papadakis, I., 1993, ApJ, 414, L85
 Manners, J., Almaini, O. & Lawrence, A. 2002, MNRAS, 330, 390
 Marconi, M., Risaliti, G., Gilli, R. et al. 2004, MNRAS, 351, 169
 Markowitz, A. & Edelson, R. 2004, ApJ, 617, 939
 Mateos, S., Barcons, X., Carrera, F.J. et al. 2005, A&A, 444, 79
 Mateos, S., Barcons, X., Carrera, F.J. et al. 2007, A&A, 473, 105
 McHardy, I.M., Papadakis, I.E., Uttley, P., Page, M.J. & Mason, K.O. 2004, MNRAS, 348, 783
 McHardy, I.M., Koering, E., Knigge, C., Uttley, P. & Fender, R.P. 2006, Nature, 444, 730
 McLure, R.J. & Dunlop, J.S. 2004, MNRAS, 352, 1390
 Nandra, K., George, I.M., Mushotzky, R.F. et al. 1997, ApJ, 476, 70
 Nikolajuk, M., Papadakis, I.E. & Czerny, B. 2004, MNRAS, 350, L26
 Nikolajuk, M., Czerny, B., Ziolkowski, J. & Gierlinski, M. 2006, MNRAS, 370, 1534
 O’Neil, P.M., Nandra, K., Papadakis, I. et al. 2005, MNRAS, 358, 1405
 Paolillo, M., Schreier, E.J., Giacomini, R. et al. 2004, ApJ, 611, 93
 Papadakis, I. E. 2004, MNRAS, 348, 207
 Ptak, A., Yaqoob, T., Mushotzky, R., Serlemitsos, P. & Griffiths, R., 1998, ApJ, 501, 37L
 Turner, T.J., George, I.M., Nandra, K. et al. 1999, ApJ, 524, 667
 Vaughan, S., Edelson, R., Warwick, R.S. et al. 2003, MNRAS, 345, 1271

Appendix

When dealing with variability, one of the main concerns is the possible contribution to the observed variations of systematic effects due to instrumental response and background. Subtle variations of these instrumental quantities may remain uncorrected and can be difficult to spot. In order to verify that no systematic instrumental variations are introducing artifacts in the light curves we use in this work, we divided the light curve of each one of the V-objects (in the observer’s frame) over its mean. Fig. 5 shows these “normalized” light curves. Most of the V-objects were mainly observed during the first five and the last three of the 10 *XMM-Newton* observations listed in Table 2. This is due to the facts that a) we chose objects with $N_{\text{data}} \geq 4$ and b) the shift between the pointing coordinates of the October 23 and 25 observations and the coordinates of the other eight observations is quite large.

We then estimated the mean of all the normalized count rates within each observation (the “mean normalized count rate” of the *XMM-Newton* observations are listed in the second column of Table 3). If there are any significant biases introduced by instrumental effects in any of the *XMM-Newton* observations, we would expect the respective mean normalized count rate to be significantly different than unity. It is only during the October 23 observation that we observe the mean to be higher than unity, but even in this case this difference is significant at the 2.5σ level only. This

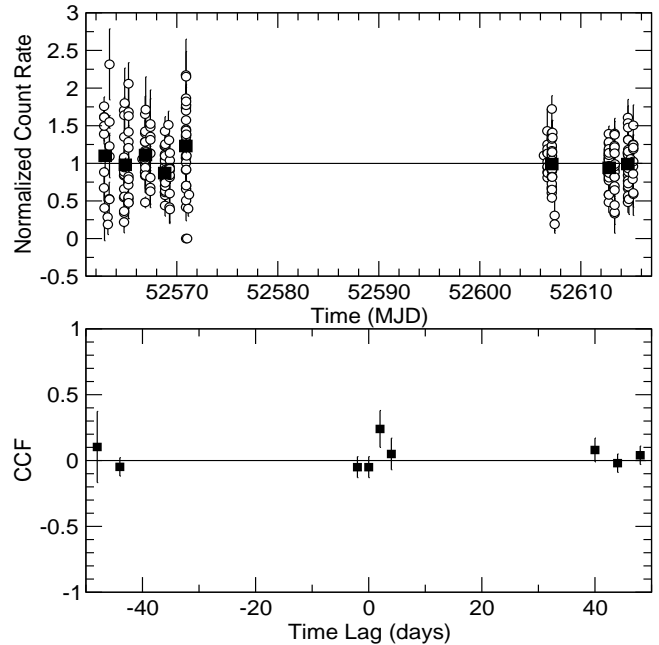


Fig. 5. Top panel: The normalized light curves of all the “V” objects in our sample (open circles). Time is in Modified Julian Days. For clarity reasons, we have changed the x-coordinates randomly, by a small amount. Filled squares show the mean of all the points within each observation (errors are also plotted, but are smaller than the symbol’s size). Bottom panel: The average CCF between source V148 and the light curves of all the other “V” sources (in the observer’s frame).

result suggests that instrumental effects do not affect significantly the observed light curves.

This conclusion is further strengthened when we consider the cross correlation between the light curves of the “V” sources in our sample. In the bottom panel of Fig. 5 we show the average cross-correlation function (CCF) between the V148 source and all the other V-sources (V148 is the brightest among the variable sources with $N_{\text{data}} = 8$). To construct this average CCF we computed first the individual CCFs between the V148 and the other sources, using light curves in the observer’s frame, the DCF method of Edelson & Krolik (1988) and a lags bin of 2 days. We then computed the mean CCF at each lag where there were more than 10 individual CCF estimates. There is no obvious significant structure in the average CCF, which is rather flat, and consistent with zero at all lags. We reached the same result when we constructed the average CCFs using a few other “reference sources”. We therefore conclude that any unaccounted instrumental effects should not contribute significantly to the variations we observe in the V-sources light curves.

The third column of Table 3 lists the “root mean square (rms) variability amplitude”, F_{var} , of all the normalized count rates within each observation and its error (which accounts only for the effects of the flux measurement errors). Both the rms variability amplitude and its error have been estimated as in Vaughan et al. (2003). In effect, F_{var} measures the scatter of all the normalized count rates around their mean within each observation. In theory, we should expect that F_{var} should remain roughly constant: we can

Table 3. The mean normalized count rate of all the “V” objects in each *XMM-Newton* observation, and the corresponding fractional root mean square variability amplitude, F_{var} .

Obs	Mean	F_{var}
2002-10-15	1.10(± 0.16)	0.51(± 0.05)
2002-10-17	0.98(± 0.09)	0.44(± 0.05)
2002-10-19	1.11(± 0.04)	0.15(± 0.04)
2002-10-21	0.87(± 0.05)	0.25(± 0.03)
2002-10-23	1.23(± 0.09)	0.35(± 0.03)
2002-11-27	0.99(± 0.04)	0.25(± 0.02)
2002-12-04	0.94(± 0.04)	0.24(± 0.02)
2002-12-06	0.99(± 0.04)	0.24(± 0.02)

consider the flux measurements of the various V-sources in each frame as an ensemble of different measurements of the same object. If the variability process is stationary, then we would not expect the rms variability amplitude to change significantly. However, this is meant to hold “on average”, as F_{var} measurements from individual light curves of an object can easily vary by a factor up to ~ 3 (see for example the bottom two panels in Fig. 6 of Vaughan et al., 2003).

The values listed in Table 3 show that F_{var} varies by a factor of $\sim 2 - 3$ from one observation to the other. It is difficult to understand how any instrumental effects could introduce such a scatter in the F_{var} values. However, even if this scatter in the F_{var} values is the result of the red-noise character of the X-ray variability in AGN, we considered the possibility it may affect the excess variance we measure for the faintest objects in our sample. For that reason, we estimated the average F_{var} of the 15 brightest and faintest objects in the V-sample. More than 10 of them were detected during the October 17 and 23 observations (which show large $F_{\text{var, total}}$ values). We find that $F_{\text{var, bright, Oct. 17}} = 0.41 \pm 0.05$ and $F_{\text{var, bright, Oct. 23}} = 0.38 \pm 0.05$, while $F_{\text{var, faint, Oct. 17}} = 0.35 \pm 0.11$ and $F_{\text{var, faint, Oct. 23}} = 0.28 \pm 0.10$. Given the fact that the fainter objects show smaller scatter around their mean, we are confident that instrumental effects do not introduce significant “artificial” variations in the light curves we use in this work.